

JGR Atmospheres

RESEARCH ARTICLE

10.1029/2023JD039679

Key Points:

- The dust storms influencing the YRD region have different transport pathways and impacting atmospheric layers
- The enlarged mass ratio of sulfate to nitrate in fine particles makes the deliquescence phenomenon appear more in dust-influence periods
- Aerosol scattering Ångström exponent is an important factor to estimate optical hygroscopicity parameters

Supporting Information:

Supporting Information may be found in the online version of this article.

Correspondence to:

Y. Wang,
yuyingwang@nuist.edu.cn

Citation:

Song, X., Wang, Y., Huang, X., Wang, Y., Li, Z., Zhu, B., et al. (2023). The Impacts of dust storms with different transport pathways on aerosol chemical compositions and optical hygroscopicity of fine particles in the Yangtze River Delta. *Journal of Geophysical Research: Atmospheres*, 128, e2023JD039679. <https://doi.org/10.1029/2023JD039679>

Received 21 JUL 2023

Accepted 8 DEC 2023

Author Contributions:

Conceptualization: Xiaorui Song
Funding acquisition: Yuying Wang, Zhanqing Li
Methodology: Xiaorui Song, Xin Huang, Rongmin Ren, Rui Zhang, Puning Zhan
Supervision: Yuying Wang
Writing – original draft: Xiaorui Song, Yuying Wang
Writing – review & editing: Xin Huang, Yuxiang Wang, Zhanqing Li, Bin Zhu, Junlin An, Jiade Yan, Yi Shang

The Impacts of Dust Storms With Different Transport Pathways on Aerosol Chemical Compositions and Optical Hygroscopicity of Fine Particles in the Yangtze River Delta

Xiaorui Song¹, Yuying Wang¹ , Xin Huang¹, Yuxiang Wang¹, Zhanqing Li² , Bin Zhu¹ , Rongmin Ren³, Junlin An¹, Jiade Yan¹, Rui Zhang¹, Yi Shang¹, and Puning Zhan¹

¹Key Laboratory for Aerosol–Cloud Precipitation of China Meteorological Administration/Special Test Field of National Integrated Meteorological Observation, Nanjing University of Information Science & Technology, Nanjing, China, ²Earth System Science Interdisciplinary Center, Department of Atmospheric and Oceanic Science, University of Maryland, College Park, MD, USA, ³State Key Laboratory of Remote-Sensing Science, College of Global Change and Earth System Science, Beijing Normal University, Beijing, China

Abstract Aerosol physicochemical properties during two dust storms (DS1: March 30–31, and DS2: May 7–8) are measured in 2021 in Nanjing, aiming to investigate the impacts of dust storms on aerosol chemical compositions and optical hygroscopicity in the Yangtze River Delta (YRD). During DS1, the dust air masses are transported in the lower atmosphere and pass through the inlands and sea areas before reaching the YRD region. During DS2, the dust air masses are transported in the upper atmosphere and pass through the inlands only. Both of them are accompanied by an increase in black carbon (BC) mass fraction and a decrease in nitrate mass fraction in fine particles (PM_{2.5}, particles with diameters less than 2.5 μm) near the surface. However, the impacts on the mass fractions of organics or sulfate are adverse between DS1 and DS2. During dust-influence periods the enlarged mass ratios of sulfate to nitrate (greater than 4) promote the occurrence of deliquescent behavior of ambient aerosols although dust aerosols can significantly suppress aerosol optical hygroscopicity. To improve model simulations of aerosol optical hygroscopicity, it is necessary to use a segment parameterization to describe aerosol light scattering enhancement factor during dust-influence periods. The closure study of optical hygroscopicity parameters with two different methods reveals the impact of aerosol scattering Ångström exponent on the estimation of optical hygroscopicity parameter. The results highlight that the impact of dust storms on aerosol chemical compositions and optical hygroscopicity are different for DS events with different transport pathways.

Plain Language Summary Dust storm (DS) is one of the severest natural disasters. Studying the change of aerosol properties during DS is important to understand the role of dust in the earth-atmosphere system. This study chooses two DS events (DS1 and DS2) in March and May 2021 to investigate the impacts of DS on aerosol chemical compositions and optical hygroscopicity in the YRD region. It is found that DS1 transporting in the lower atmosphere makes a larger increase of coarse-mode particles near the surface than DS2 transporting in the upper atmosphere. The weak impact of DS2 on the surface aerosols leads to a small change in aerosol chemical compositions of fine particles near the surface. The enlarged mass ratio of sulfate to nitrate (greater than 4) during dust periods can promote ambient aerosol deliquescence, which is important to quantify aerosol optical properties. To provide a reference for improving the model simulation of aerosol optical hygroscopicity, different parameterization schemes are derived to fit the change of aerosol light scattering enhancement factor with RH during dust and no-dust periods. The closure study of aerosol optical hygroscopicity parameters suggests that aerosol scattering Ångström exponent plays an important role in the overestimation of optical hygroscopicity parameters.

1. Introduction

As one of the severest natural disasters, dust storms (DS) have posed a great threat to atmospheric environment in the world. Dust aerosols from DS are one of the most important particulate components in the atmosphere, and they have a profound impact on air quality, human health, marine biogeochemical cycle, and climate change (Bi et al., 2016; Chen et al., 2021). The generation of DS is closely related to meteorological conditions. Strong winds can eject a large amount of dust particles from the surface to the atmosphere and transmit these dust particles, which occur mainly in arid regions (Chen et al., 2013; Nabat et al., 2015). The transport pathways and

influence areas of DS can be determined based on satellite observations or the analysis of air backward trajectories (Gandham et al., 2022; Xu et al., 2022; Yu et al., 2019).

In past decades, many studies focus on the impact of DS on air quality. Dust particles blend with anthropogenic pollutants and absorb various gases traced in the downwind path (Geng et al., 2009; Huang, Zhuang, Li, et al., 2010; Krueger et al., 2004; Li and Shao, 2012). Dust aerosols in the atmosphere can provide reactive surfaces for many heterogeneous chemical reactions during their long-distance transport (Bauer et al., 2004). Denjean et al. (2016), Huang, Zhuang, Lin, et al. (2010), and Krueger et al. (2004) demonstrate that the transport pathways, concentrations of gaseous precursors, and meteorological conditions are the main factors influencing the aging processes of dust aerosols. The secondarily generated materials (such as sulfate, nitrate, etc.) through the heterogeneous reactions can form a hydrophilic layer on the dust surface (Xu et al., 2020). Therefore, studying the change of aerosol chemical and optical hygroscopicity properties during DS is important to understand the role of dust in the earth-atmosphere system. However, studies on this are rare.

Chen et al. (2020) indicated that the optical hygroscopicity of dust aerosols plays an important role in their effects on atmospheric chemistry and climate change. The aerosol light scattering enhancement factor, $f(\text{RH})$, is defined as the ratio of scattering coefficients at a certain high relative humidity (RH) and at a relatively dry state (low RH), which is widely used to describe aerosol optical hygroscopicity. Aerosol chemical compositions and mixing state determine aerosol population hygroscopicity, which has an influence on $f(\text{RH})$. When aerosols contain a large number of dust particles, the increase of $f(\text{RH})$ with RH becomes slower due to the suppressed aerosol hygroscopicity by dust components (Xia et al., 2019). More study about the impact of dust aerosols on $f(\text{RH})$ is needed to make the quantitative analysis in the model.

In early 2021, Southeast Mongolia and North China experienced several severe DS, which seriously deteriorated air quality and reduced atmospheric visibility (Liu et al., 2021). Yin et al. (2022) identified that a sharp change in the surface air temperature and a lack of precipitation in the dust source areas resulted in dry soil and exiguous spring vegetation. The development and movement of Mongolian cyclones easily blew and transported large amounts of dust particles into North China, leading to large-scale DS (Xu et al., 2022). The severe DS can influence the Yangtze River Delta (YRD) region. In this study, two DS in March and May 2021 are selected to investigate the impacts of DS on aerosol chemical compositions and optical hygroscopicity in the YRD.

This paper is organized as follows. Section 2 describes the sampling site, the measurement instruments, and the data analysis method. Section 3 presents the analysis results, including aerosol chemical and optical properties and the relationship between aerosol chemical compositions and optical hygroscopicity during the dust and no-dust periods. A summary and conclusions are given in Section 4.

2. Materials and Methods

2.1. Sampling Site

One and a half years of comprehensive field campaign in 2020–2021 is carried out in Nanjing to study the interactions of atmosphere, aerosol, boundary layer, and cloud. Nanjing is located in the central Yangtze River Delta (YRD) (Figure 1a). The observation site is located on the campus of Nanjing University of Information Science & Technology (NUIST, 32°13'N, 118°46'E), which is surrounded by residential areas and farm lands (Figure 1b). Longwang Mountain is located on the south side of the campus. On the farther east side, there are some industrial manufacturers including steel works and power plants. In addition, two main roads (Jiangbei Blvd Expressway and Nanjing Ring Freeway) are located on the east and west sides of the campus, respectively. H. Wang et al. (2016) indicated that this site is influenced by multiple local and regional pollution sources, consisting of mineral dust, coal combustion, traffic emissions, biomass burning, and sea salts. For the YRD region, the major $\text{PM}_{2.5}$ species are organic carbon (OC), elemental carbon (EC), and water-soluble inorganic ions (K^+ , NH_4^+ , Cl^- , NO_3^- , and SO_4^{2-}) (Ming et al., 2017).

2.2. Instruments

In this campaign, two multi-wavelength integrating nephelometers (model Aurora-3000, Ecotech) are used to observe aerosol scattering coefficients (σ_{sp}) and backward scattering coefficients (σ_{bp}) at wavelengths (λ) of 450 nm, 525 nm, and 635 nm (Ren et al., 2021). A $\text{PM}_{2.5}$ cyclone inlet (BGI-VSCC) is installed at about 4 m above the ground to only let particles with diameters less than 2.5 μm ($\text{PM}_{2.5}$) enter the dual-nephelometer system, which is produced by Beijing Met High-Tech Co., Ltd. The setup of this kind of humidified nephelometer is

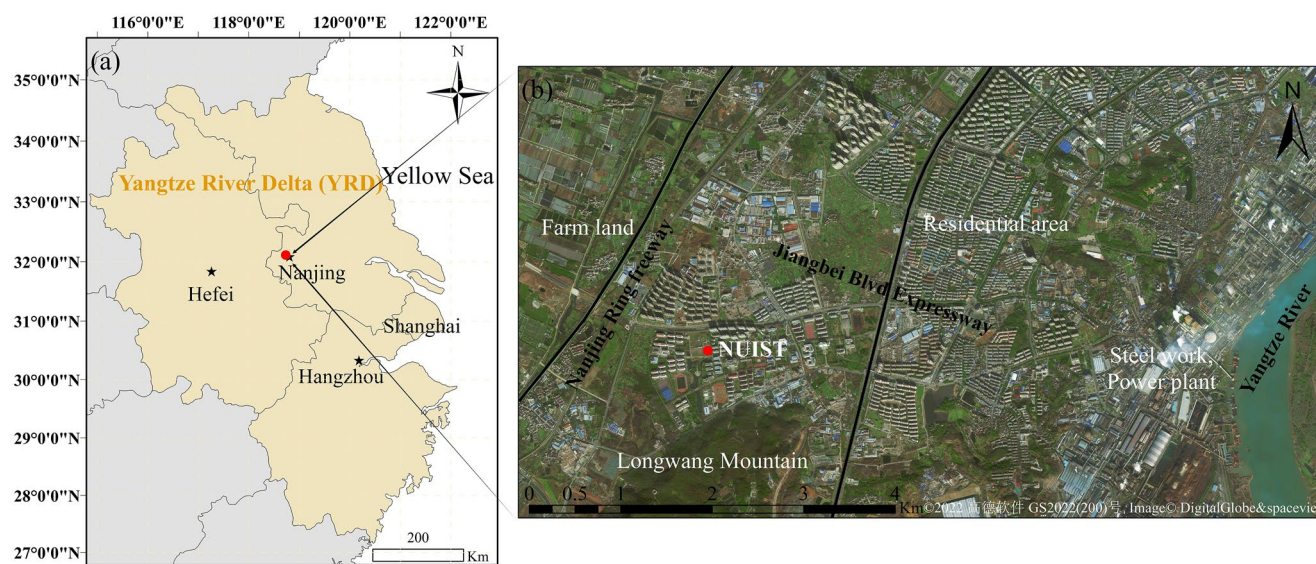


Figure 1. (a) Geographical location of Nanjing in the Yangtze River Delta and (b) the surrounding areas around the sampling site (NUIST).

first described by Kuang et al. (2017). The RH in the first nephelometer during the observation period is always controlled below 40% (Figure S1 in Supporting Information S1). An example of a whole-day RH cycle to show the performance of the system is given in Figure S2 in Supporting Information S1. Parallel experiments of two nephelometers are conducted before the field campaign, and the results are shown in Figure S3 in Supporting Information S1. It shows the good measurement consistency between two nephelometers. The optical chamber interiors of nephelometers are cleaned and full calibration is conducted every month. Full calibration is first with freon standard gas (R134) for span check, and then with dry and clean air for zero check. The calibration tolerance of the zero checks is $\pm 2 \text{ Mm}^{-1}$, and that of the span check is $\pm 2\%$ of the span point. Note that the measured σ_{sp} values and the $f(\text{RH})$ calculations are corrected for angular truncation errors, which are proposed by Müller et al. (2011).

An Aerodyne aerosol chemical speciation monitor with a quadrupole mass spectrometer and a $\text{PM}_{2.5}$ lens system (Q-ACSM) is used to measure the mass concentrations of non-refractory aerosol chemical species (sulfate, nitrate, ammonium, chloride, and organics (Org)) (Y. Wang et al., 2021). Refractory black carbon (BC) in $\text{PM}_{2.5}$ is measured using a seven-wavelength aethalometer (model AE-33, Magee), whose wavelength channels include 370, 470, 520, 590, 660, 880, and 950 nm. The mass concentration of BC is calculated from the change in optical attenuation at channel 6 (i.e., 880 nm). The retrieve of BC mass concentration at this channel is weakly affected by brown carbon and dust aerosols (Koven and Fung, 2006; Yang et al., 2009). Moreover, a micro pulse lidar (model MPL-4B, Sigma Space) is used to measure the vertical distributions of aerosol backward scattering coefficient and the depolarization ratio (DR). The DR can be used to indicate particle shapes and types (Liu et al., 2017). Due to the incomplete laser pulse, there is a dead zone of 150 m above the surface, and the maximum detection height is 20 km. A scanning mobility particle sizer (SMPS) equipped with a differential mobility analyzer (model 3081, TSI Inc.) and a condensation particle counter (model 3776, TSI Inc.) is used to measure particle number size distribution (PNSD) from 14 to 740 nm. Meteorological parameters including temperature, RH, and wind direction and speed (WD and WS) are recorded by the meteorological observatory at NUIST.

In addition to the field measurement data at NUIST, the data of $\text{PM}_{2.5}$ and particles with diameters less than $10 \mu\text{m}$ (PM_{10}) at the nearest environmental monitoring site (Maigaoqiao site) are used in this study (Figure S4 in Supporting Information S1). The Jiangsu city air quality monitor data release platform (<https://air.cnemc.cn:18014/>, last access: July 2023).

2.3. Methods

Aerosol light scattering enhancement factor, $f(\text{RH}, \lambda)$, is commonly used to characterize the impact of aerosol hygroscopicity on the aerosol scattering ability (i.e., aerosol optical hygroscopicity), which is defined as

$$f(\text{RH}, \lambda) = \frac{\sigma_{\text{sp}}(\text{RH}, \lambda)}{\sigma_{\text{sp}}(\text{RH}_0, \lambda)}, \quad (1)$$

where $\sigma_{\text{sp}}(\text{RH}, \lambda)$ denotes the scattering coefficient (σ_{sp}) at a certain high RH (RH > 40%), and $\sigma_{\text{sp}}(\text{RH}_0, \lambda)$ denotes the σ_{sp} at a certain RH₀ (RH = 0%) at the wavelength λ . The formula ($f(\text{RH})_{\text{measure}} = f(\text{RH})/f(\text{RH}_0)$) is used to correct the measured $f(\text{RH}, \lambda)$ (Kuang et al., 2017). The $f(\text{RH}_0)$ is the average of all $f(\text{RH} < 40\%, \lambda)$ during the observation period.

A physically based single-parameter scheme describing the relationship of $f(\text{RH})$ and RH is proposed by Brock et al. (2016) to describe $f(\text{RH})$. The formula is written as

$$f(\text{RH}) = 1 + \kappa_{\text{sca}} \frac{\text{RH}}{100 - \text{RH}}, \quad (2)$$

where κ_{sca} is a parameter that fits $f(\text{RH})$ best.

The scattering Ångström exponent (SAE) characterizes the wavelength dependence of σ_{sp} and is calculated using the σ_{sp} data at $\lambda_1 = 635$ nm and $\lambda_2 = 450$ nm in this study based on the following equation:

$$\text{SAE} = \frac{-\log(\sigma_{\text{sp}}(\lambda_1)/\sigma_{\text{sp}}(\lambda_2))}{\log(\lambda_1/\lambda_2)}. \quad (3)$$

An ion-pairing scheme described by Gysel et al. (2007) is applied to convert ions to inorganic salts:

$$\begin{aligned} n_{\text{NH}_4\text{NO}_3} &= n_{\text{NO}_3^-}, \\ n_{\text{NH}_4\text{HSO}_4} &= \min\left(2n_{\text{SO}_4^{2-}} - n_{\text{NH}_4^+} + n_{\text{NO}_3^-}, n_{\text{NH}_4^+} - n_{\text{NO}_3^-}\right), \\ n_{(\text{NH}_4)_2\text{SO}_4} &= \max\left(n_{\text{NH}_4^+} - n_{\text{NO}_3^-} - n_{\text{SO}_4^{2-}}, 0\right), \\ n_{\text{H}_2\text{SO}_4} &= \max\left(0, n_{\text{SO}_4^{2-}} - n_{\text{NH}_4^+} + n_{\text{NO}_3^-}\right), \\ n_{\text{HNO}_3} &= 0, \end{aligned} \quad (4)$$

where n denotes the number of moles. The volume concentration for each aerosol chemical composition is calculated according to the molar mass and their density (ρ). The ρ of H_2SO_4 , $(\text{NH}_4)_2\text{SO}_4$, NH_4HSO_4 , NH_4NO_3 , BC, and Org are 1,830, 1,769, 1,780, 1,720, 1,600, and 1,200 kg/m³, respectively. Then the volume fractions of sulfate ($\text{H}_2\text{SO}_4 + (\text{NH}_4)_2\text{SO}_4 + \text{NH}_4\text{HSO}_4$), nitrate (NH_4NO_3), and weak-hygroscopicity aerosols (BC + Org) in all aerosol chemical compositions can be calculated.

Due to the $f(\text{RH})$ is determined by multiple factors including particle number size distribution (PNSD), chemical composition, density, and refractive index, Chen et al. (2014) developed an improved algorithm for retrieving aerosol hygroscopicity parameter, $\kappa_{f(\text{RH})}$, using the data of $f(\text{RH})$, PNSD, and chemical composition. The algorithm procedure is illustrated in Figure S5 and Text S1 in Supporting Information S1.

The HYSPLIT model is used to analyze air mass sources and aerosol transport pathways (Stein et al., 2015). And the Potential Source Contribution Function (PSCF) developed by Ashbaugh et al. (1985) is used to identify aerosol source on the basis of HYSPLIT model.

Unless otherwise stated, all aerosol optical parameters discussed in this study are based on the measurements at a wavelength of 525 nm. The time appeared in this study is China Standard Time (CST), which is 8 hr ahead of UTC.

3. Results and Discussion

3.1. Overview

During the long-term field campaign in 2020–2021, two dust storm events affecting the YRD region are observed. Figures 2 and 3 show the time series of meteorological parameters and aerosol properties before and during DS1

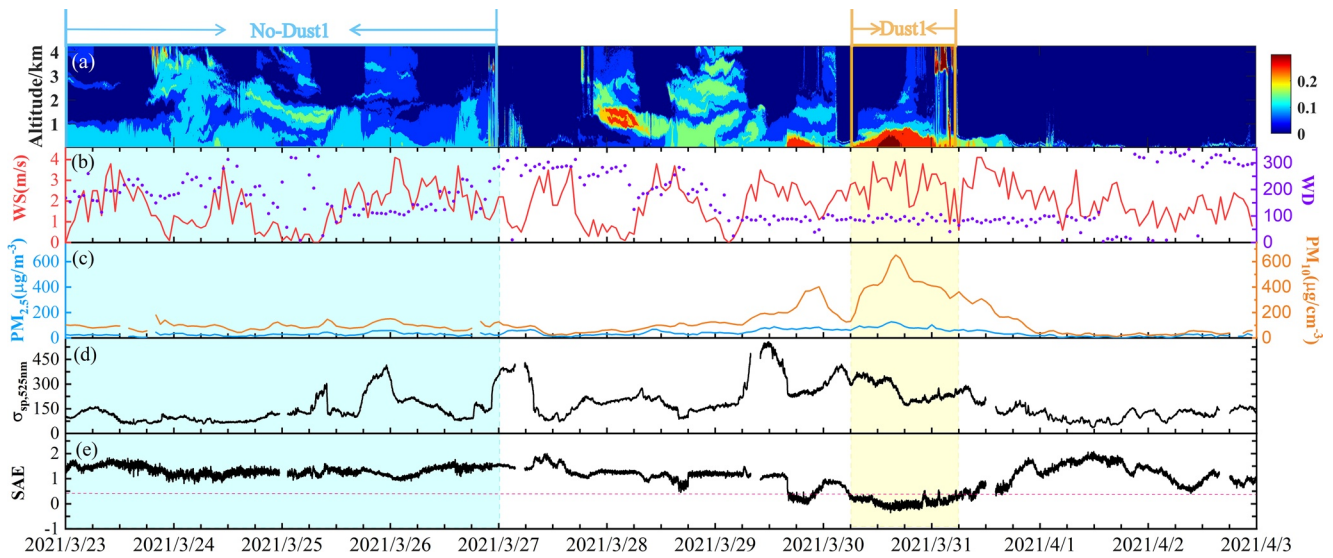


Figure 2. The time series of (a) the vertical distribution of aerosol depolarization ratio (DR), (b) hourly wind speed and direction (WS and WD), (c) mass concentrations of $PM_{2.5}$ and PM_{10} , (d) aerosol scattering coefficient (σ_{sp}) of dry aerosols at 525 nm wavelength, and (e) aerosol scattering Ångström exponent (SAE) from 23 March to 3 April 2021. All the parameters are measured at the NUIST site except for $PM_{2.5}$ and PM_{10} at the Maigaoqiao site. The blue and yellow backgrounds denote the No-Dust1 and Dust1 periods, respectively.

and DS2. The data during two dust periods [6:00 on March 30–6:00 on March 31 (Dust1) and 18:00 on May 7–18:00 on May 8 (Dust2)] and two non-dust periods [0:00 on March 23–0:00 on March 27 (No-Dust1) and 0:00 on May 1–0:00 on May 5 (No-Dust2)] are compared. The no-dust periods are selected before dust periods to avoid the impact of residual dust aerosol after the DS. In addition, several selection conditions are considered: first, the aerosol DR near the surface is less than 0.2 in the no-dust periods. Second, the meteorological conditions in selected no-dust periods are similar to those in the corresponding dust periods. Third, the time range of no-dust period is enough long to represent the general situation of no dust impact.

Zhang et al. (2021) indicated that the shape of most dust particles is nonspherical with a large DR value, ranging from 0.2 to 0.35. Figure 2a shows that the DR values near the surface remain below 0.15 during No-Dust1 and increase to above 0.2 or even 0.3 during Dust1. Moreover, the high values of DR during Dust1 are mainly found below 1 km and the surface wind speed is relatively high (Figure 2b), indicating the presence of dust

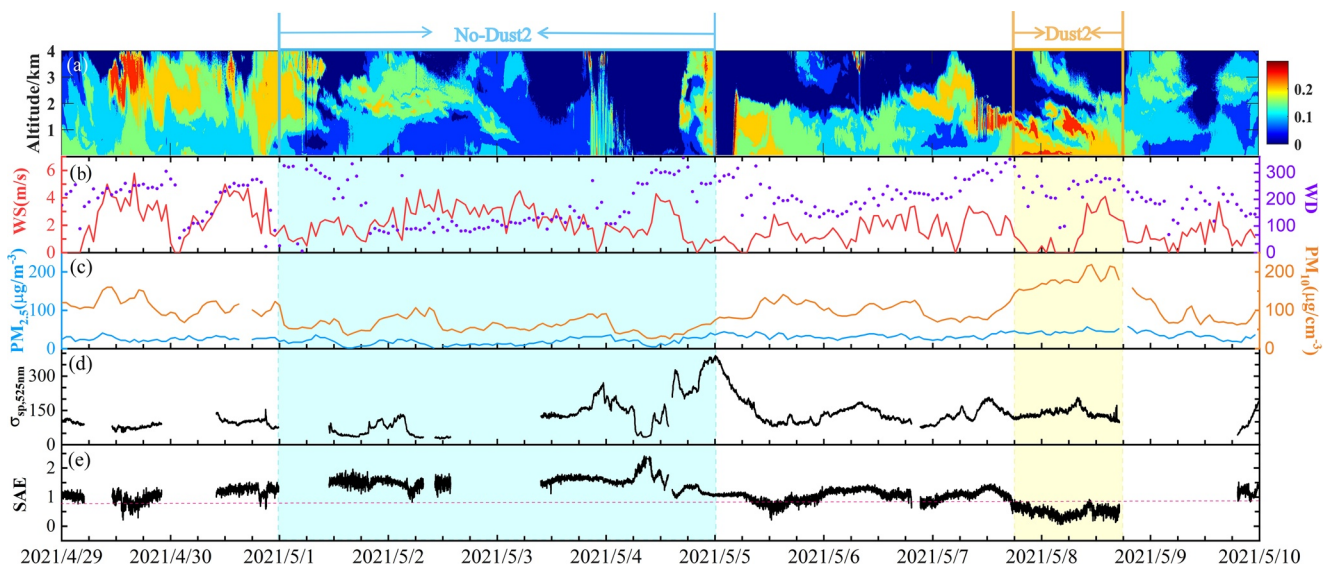


Figure 3. Same as Figure 2 but from 29 April to 10 May 2021. The blue and yellow backgrounds denote the No-Dust2 and Dust2 periods, respectively.

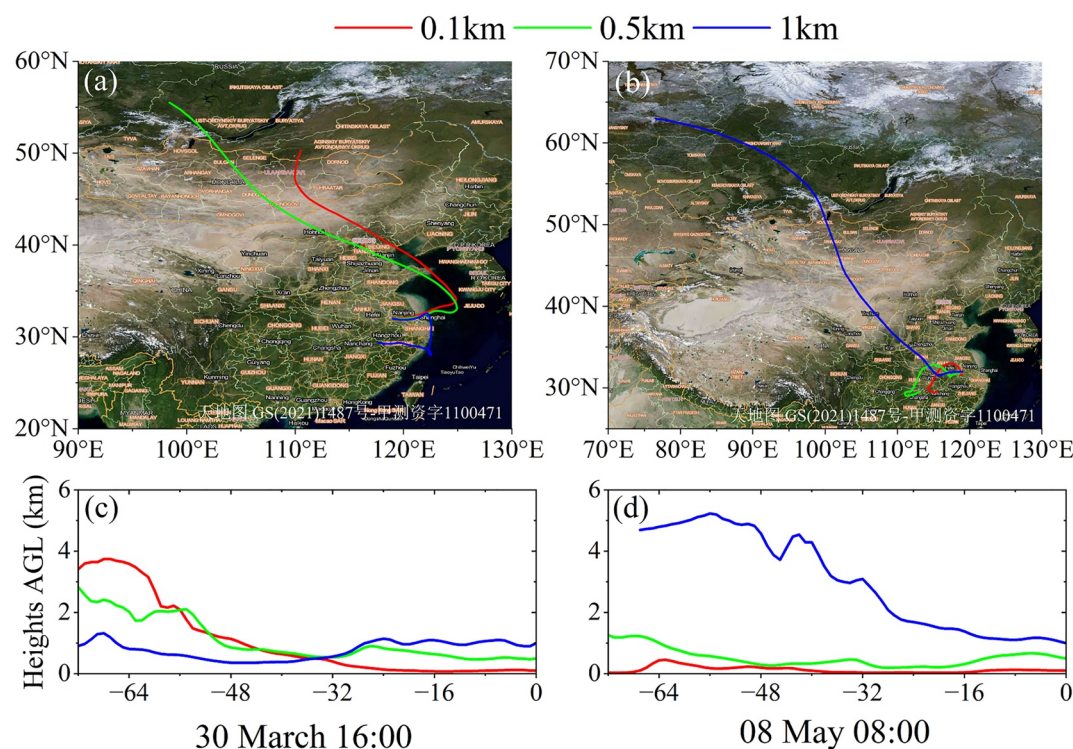


Figure 4. Seventy-two-hour HYSPLIT backward trajectories and transport heights above ground level (AGL) starting from the NUIST site at (a and c) 16:00 on March 30, and (b and d) 08:00 on 8 May 2021. The line colors show trajectories with different starting altitudes (0.1, 0.5, and 1 km).

and associated impact on aerosol properties in the lower atmosphere. Meanwhile, during No-Dust1 the mean mass concentrations of $PM_{2.5}$ and PM_{10} with the standard deviations at Maigaoqiao are 27.65 ± 11.41 and $93.06 \pm 25.52 \mu\text{g}/\text{m}^{-3}$, respectively. And they increase to 84.96 ± 19.47 and $421.92 \pm 119.82 \mu\text{g}/\text{m}^{-3}$ during Dust1 (Figure 2c). It is obvious that PM_{10} has much more increase than $PM_{2.5}$, indicating that the dust storm transports a lot of large coarse-mode dust aerosols to the YRD region. The σ_{sp} also increases during Dust1 (Figure 2d) but its trend is slightly inconsistent with that of PM_{10} or $PM_{2.5}$. This is likely because the difference in the measurement site can lead to some trend difference between σ_{sp} and PM_{10} or $PM_{2.5}$ (Figure S4 in Supporting Information S1). More importantly, the change of some aerosol properties (such as aerosol chemical composition and particle number size distribution) plays an important role in the nonlinear relationship between σ_{sp} and PM_{10} or $PM_{2.5}$ (Tao et al., 2015). This also can lead to the different trends between σ_{sp} and PM_{10} or $PM_{2.5}$. The scattering Ångström exponent (SAE) values can be used to indicate the dominated size mode of aerosols (Xia et al., 2019). The significant decrease and low values of SAE (0.08 ± 0.19) near the surface during Dust1 (Figure 2e) further indicate that the surface aerosol is impacted largely by coarse-mode particles.

Figure 3a depicts that most aerosol DR values near the surface remain below 0.15 during No-Dust2. During Dust2, the aerosol DR above 1 km altitude firstly increases above 0.2 and then that near the surface increases above 0.2. This indicates that dust aerosols during Dust2 are transported from the upper atmosphere to the YRD region, which is different from that during Dust1. This is consistent with the analysis of backward trajectories shown in Figure 4. Figure 3a also suggests that some dust aerosols in the upper atmosphere can descend to the near surface likely due to the gravitational sedimentation. During No-Dust2, the mean mass concentrations of $PM_{2.5}$ and PM_{10} with standard deviations are 16.34 ± 8.42 and $69.54 \pm 20.82 \mu\text{g}/\text{m}^{-3}$, respectively (Figure 3c). And those during Dust2 are 44.08 ± 4.65 and $178.21 \pm 20.88 \mu\text{g}/\text{m}^{-3}$, respectively. Obviously, the increases of $PM_{2.5}$ and PM_{10} are weaker during Dust2 than those during Dust1. This indicates that the dust storm with a high-altitude transport path (Dust2) has a weaker impact on the surface aerosols in the YRD region relative to that with a low-altitude transport path (Dust1). Figure 3d also suggests that the mean σ_{sp} during Dust2 ($137.13 \pm 21.28 \text{ Mm}^{-1}$) is much lower than that during Dust1 ($261.84 \pm 59.35 \text{ Mm}^{-1}$) (Figure 2d). The σ_{sp} increases slightly during the initial period of Dust2. At around 08:00 on May 8, the σ_{sp} decreases quickly with the

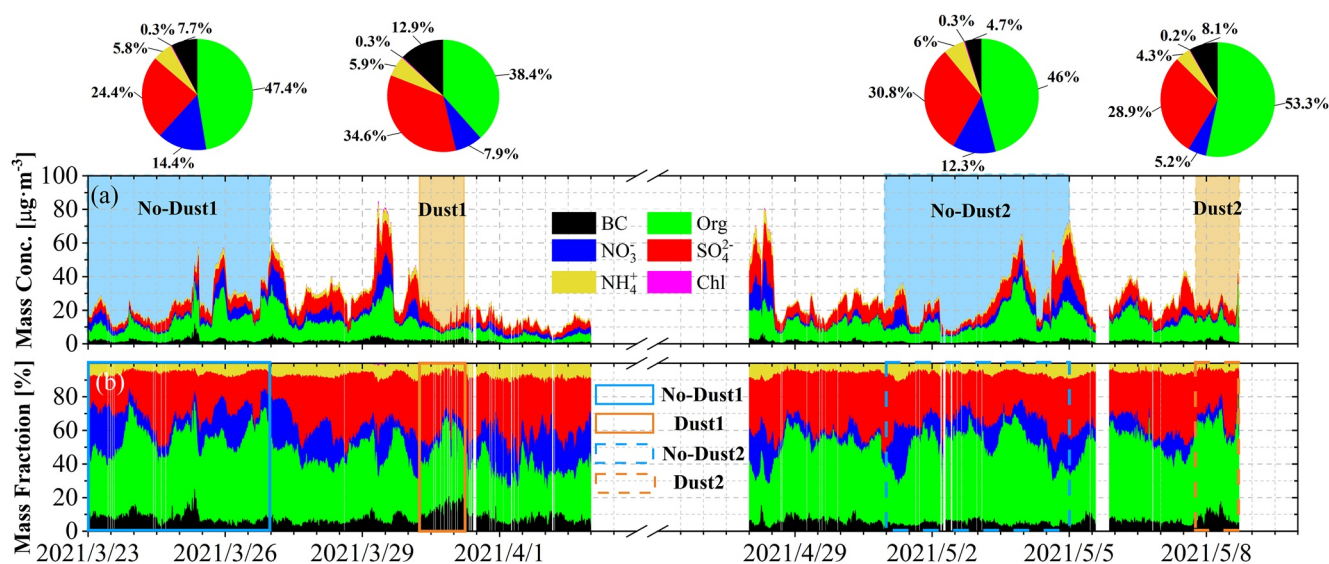


Figure 5. Time series of (a) the mass concentrations and (b) the mass fractions of aerosol chemical compositions in $PM_{2.5}$ (NO_3^- , SO_4^{2-} , NH_4^+ , Cl^- , Org, and BC). Pie charts show their mean mass fractions during No-Dust1, Dust1, No-Dust2, and Dust2.

enhancement of northwesterly winds (Figure 3b). Meanwhile, the SAE decreases from 1.56 ± 0.21 (No-Dust2) to 0.50 ± 0.14 (Dust2) (Figure 3c). All this suggests the increase of coarse-mode particles near the surface is weaker during Dust2 than that during Dust1.

Figures 4a and 4b are the seventy-two-hour HYSPLIT backward trajectories during the first dust storm (Dust1) affecting the NUIST site at 16:00 on 30 March 2021 and the second dust storm (Dust2) at 08:00 on 8 May 2021. According to the backward trajectories, both dust events originate in Mongolia, which is in agreement with previous studies (Qian et al., 2022; Xu et al., 2022). During Dust1, air masses at low altitudes (0.1 and 0.5 km) are transported long distances from Mongolia lands and pass through the sea areas before reaching the YRD region (Figure 4a). However, the air mass at the top of the boundary layer (1 km) originates from the south local inland and passes through the coast before reaching the YRD region, indicating that the upper layer is weakly affected by dust aerosols during Dust1. However, the backward trajectories during Dust2 (Figure 4b) are distinct from those during Dust1. All backward trajectories starting at three altitudes during Dust2 do not pass through the sea areas. The upper air mass (1 km) originates from Mongolia lands, while the lower air masses (0.1 and 0.5 km) originate from the southwest local inlands. This implies that dust aerosols during Dust2 mainly influence the upper atmosphere. Figures 4c and 4d also show that the initial transport heights of dust air mass in Dust2 are much higher than those of dust air masses in Dust1. These indicate that two DS have the same sources but their transport paths and impacting atmospheric layers are different.

In summary, the two DS influencing the YRD region have distinct transport paths although their sources are the same. During DS1, the dust air masses are transported in the lower atmosphere and pass through the sea areas, making a large change in aerosol properties near the surface. During DS2, the dust air masses are transported in the upper atmosphere and only pass through inlands, making a relatively weaker impact on the surface aerosol properties. Both dust air masses lead to the increase of coarse-mode particles on the surface but the increase degree is stronger during DS1.

3.2. Aerosol Chemical Compositions in $PM_{2.5}$

The time series of the mass concentrations and fractions of aerosol chemical compositions (BC, Org, NO_3^- , SO_4^{2-} , NH_4^+ , and Cl^-) in $PM_{2.5}$ are shown in Figure 5. During Dust1, the total mass concentration of aerosol chemical compositions first decreases and then increases (Figure 5a), which has similar trend with that of σ_{sp} (Figure 2d). During Dust2, the total mass concentration of aerosol chemical compositions is relatively stable. This is probably because the surface fine particles are mainly affected by the local aerosols during Dust2. Meanwhile, the low WS (Figure 3b) during the initial stage of Dust2 is not conducive to the diffusion of aerosols.

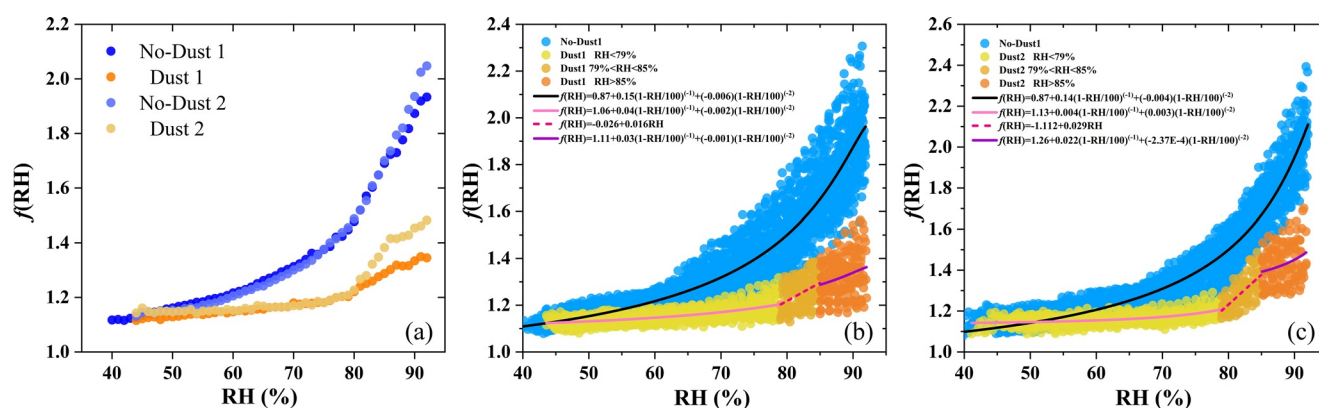


Figure 6. The variations of $f(\text{RH})$ with RH during (a) the four periods, (b) No-Dust1, Dust1 (c) No-Dust2, and Dust2. The dots in (a) represent the mean $f(\text{RH})$ at intervals of 1% RH. The dots in (b) and (c) represent the measured $f(\text{RH})$ and the lines show the fitting results using the $f(\text{RH})$ parameterization schemes.

Figure 5b shows that the mass fractions of aerosol chemical compositions have an obvious change from no-dust periods (No-Dust1 and No-Dust2) to dust periods (Dust1 and Dust2).

The pie charts in Figure 5 further suggest that the mass fractions of BC during Dust1 and Dust2 (12.9% and 8.1%) are higher than those during No-Dust1 and No-Dust2 (7.7% and 4.7%). The increased BC may be from the long-distance carrying of dust air masses from the highly populated areas in North China. The pie charts in Figure 5 also suggest the mass fractions of nitrate during dust periods are lower than those during no-dust periods, suggesting that the DS do not greatly promote the formation of nitrate. This is in contrast to a study by Z. Wang et al. (2018), which suggests that the formation of sulfate is few but the formation of nitrate is abundant through the heterogeneous reactions on the dust surface. The reason for this difference is that the heterogeneous reactions strongly depend on multiple factors, including mineralogy, RH, and the concentrations of SO_2 and NO_2 (Gaston, 2020). As an example, Krueger et al. (2004) and Xu et al. (2020) indicated that the heterogeneous reactions of mineral dust are intensely correlated with dust compositions. The calcium-containing minerals, such as calcite (CaCO_3) and dolomite ($\text{CaMg}(\text{CO}_3)_2$), are favorable for nitrate formation, while alkaline metals are favorable for sulfate formation.

The mass fraction of sulfate is larger during Dust1 than that during No-Dust1. Three possible reasons can lead to the increase of sulfate mass fraction: first, as mentioned above, a large part of dust particles are alkaline, which is in favor of the transformation of SO_2 to sulfate through the enhanced heterogeneous reactions on the surface of dust aerosols (Y. Wang et al., 2005). Second, the sulfate existing in primary dust can be transported to the YRD region (Q. Wang et al., 2011). Finally, as shown in Figure 4a, the air masses during Dust1 pass through the sea areas, which can carry sea-salt sulfate to the YRD region. During Dust2, the mass fraction of organics is higher than that during No-Dust2. The analysis of potential source contribution function (PSCF, Figure S6 in Supporting Information S1) suggests that most organics during Dust2 are mainly from local emission and regional transmission near the surface.

In summary, there are similarities and differences in the impact of DS1 and DS2 on aerosol chemical compositions in $\text{PM}_{2.5}$. In general, the retrieved BC mass fraction increases and the detected nitrate mass fraction decreases from no-dust periods to dust periods. However, the mass fraction change of organics or sulfate is adverse between from No-Dust1 to Dust1 and from No-Dust2 to Dust2. This is caused by the different transport paths of DS1 and DS2. The weaker impact of dust storm on the surface aerosols during DS2 leads to a smaller change in aerosol chemical compositions in $\text{PM}_{2.5}$.

3.3. Aerosol Light Scattering Enhancement Factor in $\text{PM}_{2.5}$

Figure 6 displays the change of $f(\text{RH})$ with RH during No-Dust1, Dust1, No-Dust2, and Dust2. The mean $f(\text{RH})$ at intervals of 1% RH during four periods is shown in Figure 6a. It indicates that the values of $f(\text{RH})$ during Dust1 and Dust2 are always less than those during No-Dust1 and No-Dust2, especially at the moderate and high RH levels. Moreover, ambient aerosol deliquescence phenomenon can be found around $\text{RH} = 79\text{--}85\%$ during Dust1 and Dust2, showing a slow increase of $f(\text{RH})$ at $\text{RH} < 79\%$ and a fast increase of $f(\text{RH})$ at $79\% < \text{RH} < 85\%$.

Ammonium sulfate and ammonium nitrate (AS-AN) particles with different mixing ratios lead to mutual deliquescence relative humidity (MDRH) and full deliquescence relative humidity (DRH). The DRH of AS-AN particles increased with the decrease of ammonium nitrate content, closing to the DRH of pure ammonium sulfate particles (Sun et al., 2018). Ren et al. (2021) showed that the environmental aerosol deliquescence phenomenon is easy to occur when the mass ratio of sulfate to nitrate ($R_{\text{SO}_4^{2-}/\text{NO}_3^-}$) is greater than ~ 4 . According to our measurement, $R_{\text{SO}_4^{2-}/\text{NO}_3^-}$ in $\text{PM}_{2.5}$ during Dust1 and Dust2 are always higher than 4 (Figure S7 in Supporting Information S1), which is the reason for environmental aerosol deliquescence during dust periods. Because of the higher $R_{\text{SO}_4^{2-}/\text{NO}_3^-}$ in Dust2 than that in Dust1, the aerosol deliquescence phenomenon is more intense during Dust2 than that during Dust1. As a contrast, $f(\text{RH})$ during No-Dust1 and No-dust2 increases rapidly with RH and the $f(\text{RH} = 90\%)$ is close to 1.9. All the results demonstrate that DS can effectively reduce aerosol optical hygroscopicity by increasing the hydrophobic aerosols (such as mineral aerosols) although they may promote the formation of secondary aerosols (Shi et al., 2008).

To improve the simulation accuracy of aerosol optical hygroscopicity, it is necessary to develop an optimal parameterization to describe $f(\text{RH})$. The following three-parameter parameterization scheme is commonly applied for no deliquescence phenomenon of environmental aerosols, which is used during No-Dust1 and No-Dust2.

$$f(\text{RH}) = a + b\left(1 - \frac{\text{RH}}{100}\right)^{-1} + c\left(1 - \frac{\text{RH}}{100}\right)^{-2} \quad (5)$$

where a , b , and c are three fitting parameters.

Due to the environmental aerosol deliquescence phenomenon during Dust1 and Dust2, the above scheme can bring a large deviation. The following segment parameterization scheme is used.

$$\begin{cases} f(\text{RH}) = a + b\left(1 - \frac{\text{RH}}{100}\right)^{-1} + c\left(1 - \frac{\text{RH}}{100}\right)^{-2} & \text{RH} < 79\% \\ f(\text{RH}) = a + b\text{RH} & 79 \leq \text{RH} \leq 85\% \\ f(\text{RH}) = a + b\left(1 - \frac{\text{RH}}{100}\right)^{-1} + c\left(1 - \frac{\text{RH}}{100}\right)^{-2} & \text{RH} > 85\% \end{cases} \quad (6)$$

where a , b , and c are the fitting parameters.

The parameterization results are shown in Figures 6b and 6c. The results also suggest that the environmental aerosol deliquescence phenomenon during Dust2 is more obvious than that during Dust1. Different aerosol characteristics in different regions cause the diverse $f(\text{RH})$ parameterization scheme (Table S2 in Supporting Information S1). As a result, the three-parameter parameterization of $f(\text{RH})$ is adapted during non-dust periods, which can be used for the simulation of aerosol optical hygroscopicity for the general situation in the Yangtze River Delta. Meanwhile, the segment parameterization is highly adapted for the special dust periods.

Figure 7 shows the $f(\text{RH} = 85\%)$ as a function of the volume fractions of aerosol chemical components during different periods. The $f(\text{RH} = 85\%)$ and the volume fraction of sulfate aerosols are always positively correlated, with higher correlation coefficients ($R = 0.69$ and 0.76) during Dust1 and Dust2 than those during No-Dust1 and No-Dust2 ($R = 0.22$ and 0.47) (Figures 7a and 7d). This indicates the enhancement effect of sulfate aerosols on aerosol optical hygroscopicity, especially during dust periods. Figures 7b and 7e show that the volume fractions of NH_4NO_3 are positively correlated with the $f(\text{RH} = 85\%)$ during Dust1, No-Dust1, and No-Dust2 ($R = 0.83$, 0.67 , and 0.23), also implying the enhancement effect of nitrate aerosols on aerosol optical hygroscopicity. However, the volume fraction of NH_4NO_3 is negatively correlated with the $f(\text{RH} = 85\%)$ during Dust2 ($R = -0.78$) (Figure 7e). This is because the decrease of nitrate is always accompanied by the rapid increase of sulfate aerosols during Dust2 (Figure S8 in Supporting Information S1), the increased sulfate aerosols make the increase of $f(\text{RH} = 85\%)$ when NH_4NO_3 decreases. This is also why the more obvious environmental aerosol deliquescence phenomenon in Dust2 than in Dust1. Figures 7c and 7f suggest that the $f(\text{RH} = 85\%)$ are always negatively correlated with the total volume fractions of weak-hygroscopicity aerosols (Org + BC) during four periods, indicating the large suppressing impact of organics and BC on aerosol optical hygroscopicity.

During the observation period, the fitted κ_{sea} using Equation 2 ranges from 0.03 to 0.15. As mentioned above, the $f(\text{RH})$ is affected by particle number size distribution (PNSD), chemical composition, and so on. Using the

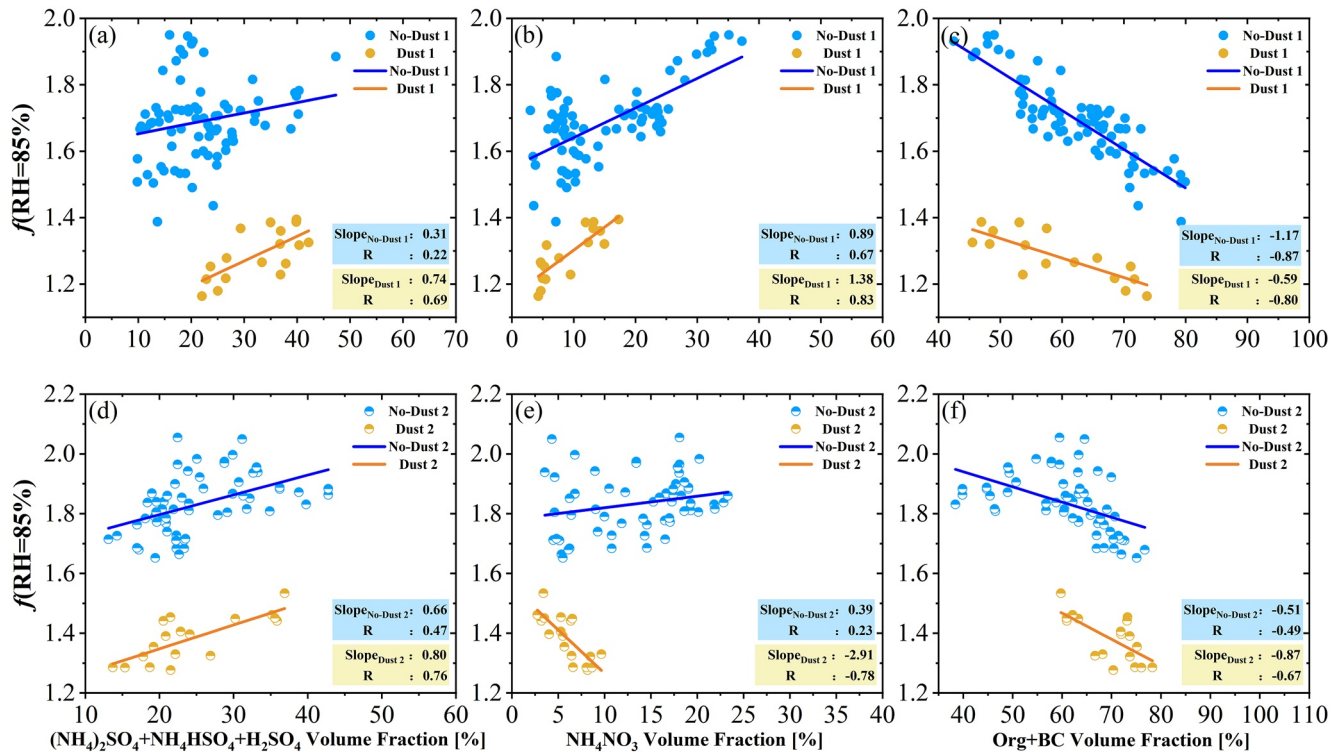


Figure 7. Aerosol light scattering enhancement factor at $RH = 85\%$, $f(RH = 85\%)$, as a function of the volume fractions of aerosol chemical components: (a and d) sulfate aerosols ($H_2SO_4 + (NH_4)_2SO_4 + NH_4HSO_4$), (b and e) nitrate aerosol (NH_4NO_3), and (c and f) weak-hygroscopicity aerosols (Org + BC) during dust and non-dust periods. Solid blue and orange lines represent bivariate regression lines.

data of PNSD and chemical components, the $f(RH)$ can be calculated based on the Mie model, and then aerosol hygroscopic parameter, $\kappa_{f(RH)}$, can be retrieved (see the method described in Section 2.3). The comparison between $\kappa_{f(RH)}$ and κ_{sca} is shown in Figures 8a and 8b. The mean ratio $\kappa_{sca}/\kappa_{f(RH)}$ (R_κ) are 0.78, 0.63, 0.75, and 0.66 in No-Dust1, Dust1, No-Dust2, and Dust2, respectively. It suggests that the calculated $\kappa_{f(RH)}$ is more approaching to κ_{sca} during no-dust periods than that during dust periods. During dust periods, the overestimation of $\kappa_{f(RH)}$ is obvious. The variation of R_κ with SAE is shown in Figure 8c. It shows that R_κ becomes lower with the decrease of SAE, indicating the large impact of PNSD difference on R_κ . This phenomenon is consistent with the report of Kuang et al. (2017). The correlation coefficient ($R^2 = 0.58$) between R_κ and SAE confirms that the variability of

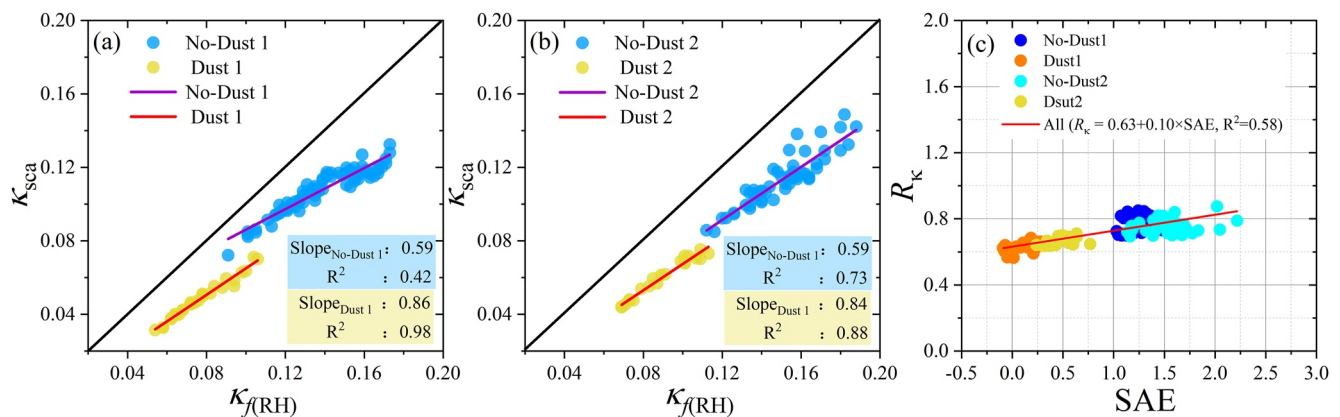


Figure 8. The linear relationship between values of $\kappa_{f(RH)}$ calculated by Mie model and κ_{sca} fitted by formula 2 during (a) No-Dust1, Dust1, (b) No-Dust2, and Dust2. Solid purple and red lines represent bivariate regression lines. The black line is a 1:1 line. (c) The ratio $\kappa_{sca}/\kappa_{f(RH)}$ (R_κ) versus SAE during Dust1, Dust2, No-Dust1, and No-Dust2. The red line represents the linear fit.

R_k can be mostly explained by the change of SAE. The parameterization scheme between R_k and SAE in this study is $R_k = 0.63 + 0.10 \times \text{SAE}$, which is different with that proposed by Yu et al. (2018) ($R_k = 0.45 + 0.15 \times \text{SAE}$). This is likely related to the difference of aerosol chemical compositions between two different measurement sites. The non-detected dust aerosols can also lead to the overestimation of $\kappa_{f(\text{RH})}$. However, the content of dust aerosols is small in fine particles.

In summary, the DS can significantly suppress aerosol optical hygroscopicity in the YRD region. The enlarged $R_{\text{SO}_4^{2-}/\text{NO}_3^-}$ (larger than 4) promotes environmental aerosol deliquescence during dust periods. The relationships between $f(\text{RH} = 85\%)$ and aerosol chemical components highlight the enhancement effect of sulfate and nitrate aerosols and the suppressing effect of weak-hygroscopicity aerosols on aerosol optical hygroscopicity. The closures between $\kappa_{f(\text{RH})}$ and κ_{sca} further indicate that the low SAE is responsible for the overestimation of $\kappa_{f(\text{RH})}$ during dust periods. To accurately parameterize $f(\text{RH})$, dust and no-dust periods need to be distinguished.

4. Conclusions and Impactions

In this study, two DS (DS1 and DS2) are chosen to study the impacts of DS on aerosol chemical compositions and optical hygroscopicity based on the field measurements in Nanjing in 2021. The data during two dust periods [6:00 on March 30–36:00 on March 31 (Dust1) and 18:00 on 7 May–18:00 on 8 May (Dust2)] and two no-dust periods [0:00 on 23 March–0:00 on 27 March (No-Dust1) and 0:00 on 1 May–0:00 on 5 May (No-Dust2)] are selected to compare.

The seventy-two-hour HYSPLIT backward trajectories suggest that two DS have different transport paths and different impacting atmospheric layers, making a different change in the chemical components and optical hygroscopicity of aerosols near the surface. During DS1, the dust air masses are transported in the lower atmosphere and pass through the inlands and sea areas before reaching the YRD region. During DS2, the dust air masses are transported in the upper atmosphere and only pass through the inlands. As a result, DS1 has a stronger impact on aerosol properties near the surface than DS2. Both DS1 and DS2 lead to increases in coarse-mode particles near the surface but the increasing degree is higher in DS1 than in DS2.

The measurements by ACSM and AE-33 show that the black carbon (BC) mass fraction increases and the nitrate mass fraction decreases in fine particles ($\text{PM}_{2.5}$) from no-dust periods to dust periods. However, a change in the mass fraction of organics or sulfate is adverse between two dust periods compared to two no-dust periods, which is caused by the different transport paths and impacting heights of DS. The weaker impact of dust storm on the surface aerosols during Dust2 leads to a smaller change of aerosol chemical compositions near the surface.

The variation of aerosol light scattering enhancement factor ($f(\text{RH})$) with RH indicates that dust aerosols can effectively reduce aerosol optical hygroscopicity. Meanwhile, the sulfate and nitrate aerosols have the enhancement effect and the organics and BC aerosols have the suppressing effect on aerosol optical hygroscopicity. The enlarged mass ratio of sulfate to nitrate (greater than 4) during dust periods can promote environmental aerosol deliquescence. For this reason, a three-parameter parameterization scheme to fit $f(\text{RH})$ is reasonable to no-dust periods, while a segment parameterization scheme is reasonable to dust periods. The founded environmental aerosol deliquescence phenomena in dust periods are special in this study, which inspires scientists to think deeply the impact of dust aerosols on atmospheric environment.

The closure study between the $\kappa_{f(\text{RH})}$ calculated by Mie model and κ_{sca} fitted by measured $f(\text{RH})$ suggests that the variability of R_k can be mostly explained by the change of SAE. More research about the factors for optical hygroscopicity parameters are needed in the future. To accurately parameterize $f(\text{RH})$, dust and no-dust periods need to be distinguished in models.

Conflict of Interest

The authors declare no conflicts of interest relevant to this study.

Data Availability Statement

Data availability may be found in the online version of this article. The data used in the analysis are available at DOI: <https://doi.org/10.57760/sciencedb.09680>. HYSPLIT trajectories are available via the READY website by the NOAA (<https://www.ready.noaa.gov>; NOAA, 2022).

Acknowledgments

We thank the funding from the National Natural Science Foundation of China (NSFC) research project (42030606, 42005067, 92044303). We also thank the China meteorological administration (CMA) integrated meteorological observation and training center (Nanjing) for providing the meteorological data.

References

- Ashbaugh, L. L., Malm, W. C., & Sadeh, W. Z. (1985). A residence time probability analysis of sulfur concentrations at grand Canyon National Park [Software]. *Atmospheric Environment*, *19*(8), 1263–1270. [https://doi.org/10.1016/0004-6981\(85\)90256-2](https://doi.org/10.1016/0004-6981(85)90256-2)
- Bauer, S. E., Balkanski, Y., Schulz, M., Hauglustaine, D. A., & Dentener, F. (2004). Global modeling of heterogeneous chemistry on mineral aerosol surfaces: Influence on tropospheric ozone chemistry and comparison to observations. *Journal of Geophysical Research*, *109*(D2). <https://doi.org/10.1029/2003JD003868>
- Bi, J., Huang, J., Holben, B., & Zhang, G. (2016). Comparison of key absorption and optical properties between pure and transported anthropogenic dust over East and Central Asia. *Atmospheric Chemistry and Physics*, *16*(24), 15501–15516. <https://doi.org/10.5194/acp-16-15501-2016>
- Brock, C. A., Wagner, N. L., Anderson, B. E., Attwood, A. R., Beyersdorf, A., Campuzano-Jost, P., et al. (2016). Aerosol optical properties in the southeastern United States in summer – Part 1: Hygroscopic growth. *Atmospheric Chemistry and Physics*, *16*(8), 4987–5007. <https://doi.org/10.5194/acp-16-4987-2016>
- Chen, F., Qiang, M., Zhou, A., Xiao, S., Chen, J., & Sun, D. (2013). A 2000-year dust storm record from Lake Sugan in the dust source area of arid China. *Journal of Geophysical Research: Atmospheres*, *118*(5), 2149–2160. <https://doi.org/10.1002/jgrd.50140>
- Chen, J., Zhao, C. S., Ma, N., & Yan, P. (2014). Aerosol hygroscopicity parameter derived from the light scattering enhancement factor measurements in the North China Plain. *Atmospheric Chemistry and Physics*, *14*(15), 8105–8118. <https://doi.org/10.5194/acp-14-8105-2014>
- Chen, L., Peng, C., Gu, W., Fu, H., Jian, X., Zhang, H., et al. (2020). On mineral dust aerosol hygroscopicity. *Atmospheric Chemistry and Physics*, *20*(21), 13611–13626. <https://doi.org/10.5194/acp-20-13611-2020>
- Chen, S., Liu, J., Wang, X., Zhao, S., Chen, J., Qiang, M., et al. (2021). Holocene dust storm variations over northern China: Transition from a natural forcing to an anthropogenic forcing. *Science Bulletin*, *66*(24), 2516–2527. <https://doi.org/10.1016/j.scib.2021.08.008>
- Denjean, C., Cassola, F., Mazzino, A., Triquet, S., Chevaillier, S., Grand, N., et al. (2016). Size distribution and optical properties of mineral dust aerosols transported in the western Mediterranean. *Atmospheric Chemistry and Physics*, *16*(2), 1081–1104. <https://doi.org/10.5194/acp-16-1081-2016>
- Gandham, H., Dasari, H. P., Karumuri, A., Ravuri, P. M. K., & Hoteit, I. (2022). Three-dimensional structure and transport pathways of dust aerosols over West Asia. *npj Climate and Atmospheric Science*, *5*(1), 45. <https://doi.org/10.1038/s41612-022-00266-2>
- Gaston, C. J. (2020). Re-Examining dust chemical aging and its impacts on Earth's climate. *Accounts of Chemical Research*, *53*(5), 1005–1013. <https://doi.org/10.1021/acs.accounts.0c00102>
- Geng, H., Park, Y., Hwang, H., Kang, S., & Ro, C. U. (2009). Elevated nitrogen-containing particles observed in Asian dust aerosol samples collected at the marine boundary layer of the Bohai Sea and the Yellow Sea. *Atmospheric Chemistry and Physics*, *9*(18), 6933–6947. <https://doi.org/10.5194/acp-9-6933-2009>
- Gysel, M., Crosier, J., Topping, D. O., Whitehead, J. D., Bower, K. N., Cubison, M. J., et al. (2007). Closure study between chemical composition and hygroscopic growth of aerosol particles during TORCH2. *Atmospheric Chemistry and Physics*, *7*(24), 6131–6144. <https://doi.org/10.5194/acp-7-6131-2007>
- Huang, K., Zhuang, G., Li, J., Wang, Q., Sun, Y., Lin, Y., & Fu, J. S. (2010). Mixing of Asian dust with pollution aerosol and the transformation of aerosol components during the dust storm over China in spring 2007. *Journal of Geophysical Research*, *115*(D7). <https://doi.org/10.1029/2009JD013145>
- Huang, K., Zhuang, G., Lin, Y., Li, J., Sun, Y., Zhang, W., & Fu, J. S. (2010). Relation between optical and chemical properties of dust aerosol over Beijing, China. *Journal of Geophysical Research*, *115*(D7). <https://doi.org/10.1029/2009JD013212>
- Koven, C. D., & Fung, I. (2006). Inferring dust composition from wavelength-dependent absorption in Aerosol Robotic Network (AERONET) data. *Journal of Geophysical Research*, *111*(D14). <https://doi.org/10.1029/2005JD006678>
- Krueger, B. J., Grassian, V. H., Cowin, J. P., & Laskin, A. (2004). Heterogeneous chemistry of individual mineral dust particles from different dust source regions: The importance of particle mineralogy. *Atmospheric Environment*, *38*(36), 6253–6261. <https://doi.org/10.1016/j.atmosenv.2004.07.010>
- Kuang, Y., Zhao, C., Tao, J., Bian, Y., Ma, N., & Zhao, G. (2017). A novel method for deriving the aerosol hygroscopicity parameter based only on measurements from a humidified nephelometer system. *Atmospheric Chemistry and Physics*, *17*(11), 6651–6662. <https://doi.org/10.5194/acp-17-6651-2017>
- Li, W., & Shao, L. (2012). Chemical modification of dust particles during different dust storm episodes. *Aerosol and Air Quality Research*, *12*(6), 1095–1104. <https://doi.org/10.4209/aaqr.2011.11.0188>
- Liu, B., Ma, Y., Gong, W., & Zhang, M. (2017). Observations of aerosol color ratio and depolarization ratio over Wuhan. *Atmospheric Pollution Research*, *8*(6), 1113–1122. <https://doi.org/10.1016/j.apr.2017.04.004>
- Liu, S., Xing, J., Sahu, S. K., Liu, X., Liu, S., Jiang, Y., et al. (2021). Wind-blown dust and its impacts on particulate matter pollution in Northern China: Current and future scenarios. *Environmental Research Letters*, *16*(11), 114041. <https://doi.org/10.1088/1748-9326/ac31ec>
- Ming, L., Jin, L., Li, J., Fu, P., Yang, W., Liu, D., et al. (2017). PM_{2.5} in the Yangtze River Delta, China: Chemical compositions, seasonal variations, and regional pollution events. *Environmental Pollution*, *223*, 200–212. <https://doi.org/10.1016/j.envpol.2017.01.013>
- Müller, T., Laborde, M., Kassell, G., & Wiedensohler, A. (2011). Design and performance of a three-wavelength LED-based total scatter and backscatter integrating nephelometer. *Atmospheric Measurement Techniques*, *4*(6), 1291–1303. <https://doi.org/10.5194/amt-4-1291-2011>
- Nabat, P., Somot, S., Mallet, M., Michou, M., Sevault, F., Driouech, F., et al. (2015). Dust aerosol radiative effects during summer 2012 simulated with a coupled regional aerosol–atmosphere–ocean model over the Mediterranean. *Atmospheric Chemistry and Physics*, *15*(6), 3303–3326. <https://doi.org/10.5194/acp-15-3303-2015>
- Qian, W., Leung, J. C., Ren, J., Du, J., Feng, Y., & Zhang, B. (2022). Anomaly based synoptic analysis and model prediction of six dust storms moving from Mongolia to northern China in spring 2021. *Journal of Geophysical Research: Atmospheres*, *127*(7), e2021jg036272. <https://doi.org/10.1029/2021JD036272>
- Ren, R., Li, Z., Yan, P., Wang, Y., Wu, H., Cribb, M., et al. (2021). Measurement report: The effect of aerosol chemical composition on light scattering due to the hygroscopic swelling effect. *Atmospheric Chemistry and Physics*, *21*(13), 9977–9994. <https://doi.org/10.5194/acp-21-9977-2021>

- Shi, Z., Zhang, D., Hayashi, M., Ogata, H., Ji, H., & Fujie, W. (2008). Influences of sulfate and nitrate on the hygroscopic behaviour of coarse dust particles. *Atmospheric Environment*, 42(4), 822–827. <https://doi.org/10.1016/j.atmosenv.2007.10.037>
- Stein, A. F., Draxler, R. R., Rolph, G. D., Stunder, B. J. B., Cohen, M. D., & Ngan, F. (2015). NOAA's HYSPLIT atmospheric transport and dispersion modeling system [software]. *Bulletin of the American Meteorological Society*, 96(12), 2059–2077. <https://doi.org/10.1175/BAMS-D-14-00110.1>
- Sun, J., Liu, L., Xu, L., Wang, Y., Wu, Z., Hu, M., et al. (2018). Key role of nitrate in phase transitions of urban particles: Implications of important reactive surfaces for secondary aerosol formation. *Journal of Geophysical Research: Atmospheres*, 123(2), 1234–1243. <https://doi.org/10.1002/2017JD027264>
- Tao, J., Zhang, L., Gao, J., Wang, H., Chai, F., & Wang, S. (2015). Aerosol chemical composition and light scattering during a winter season in Beijing. *Atmospheric Environment*, 110, 36–44. <https://doi.org/10.1016/j.atmosenv.2015.03.037>
- Wang, H., An, J., Cheng, M., Shen, L., Zhu, B., Li, Y., et al. (2016). One year online measurements of water-soluble ions at the industrially polluted town of Nanjing, China: Sources, seasonal and diurnal variations. *Chemosphere*, 148, 526–536. <https://doi.org/10.1016/j.chemosphere.2016.01.066>
- Wang, Q., Zhuang, G., Li, J., Huang, K., Zhang, R., Jiang, Y., et al. (2011). Mixing of dust with pollution on the transport path of Asian dust: Revealed from the aerosol over Yulin, the north edge of Loess Plateau. *Science of the Total Environment*, 409(3), 573–581. <https://doi.org/10.1016/j.scitotenv.2010.10.032>
- Wang, Y., Li, Z., Wang, Q., Jin, X., Yan, P., Cribb, M., et al. (2021). Enhancement of secondary aerosol formation by reduced anthropogenic emissions during Spring Festival 2019 and enlightenment for regional PM_{2.5} control in Beijing. *Atmospheric Chemistry and Physics*, 21(2), 915–926. <https://doi.org/10.5194/acp-21-915-2021>
- Wang, Y., Zhuang, G., Sun, Y., & An, Z. (2005). Water-soluble part of the aerosol in the dust storm season—Evidence of the mixing between mineral and pollution aerosols. *Atmospheric Environment*, 39(37), 7020–7029. <https://doi.org/10.1016/j.atmosenv.2005.08.005>
- Wang, Z., Pan, X., Uno, I., Chen, X., Yamamoto, S., Zheng, H., et al. (2018). Importance of mineral dust and anthropogenic pollutants mixing during a long-lasting high PM event over East Asia. *Environmental Pollution*, 234, 368–378. <https://doi.org/10.1016/j.envpol.2017.11.068>
- Xia, C., Sun, J., Qi, X., Shen, X., Zhong, J., Zhang, X., et al. (2019). Observational study of aerosol hygroscopic growth on scattering coefficient in Beijing: A case study in March of 2018. *Science of the Total Environment*, 685, 239–247. <https://doi.org/10.1016/j.scitotenv.2019.05.283>
- Xu, W., Kuang, Y., Liang, L., He, Y., Cheng, H., Bian, Y., et al. (2020). Dust-dominated coarse particles as a medium for rapid secondary organic and inorganic aerosol formation in highly polluted air. *Environmental Science & Technology*, 54(24), 15710–15721. <https://doi.org/10.1021/acs.est.0c07243>
- Xu, X., Zhao, P., Yin, Y., Cheng, W., Wang, J., Li, P., et al. (2022). Dust particles transport during the rare strong sandstorm process in Northern China in early year 2021. *Air Quality, Atmosphere & Health*, 15(6), 929–936. <https://doi.org/10.1007/s11869-022-01159-2>
- Yang, M., Howell, S. G., Zhuang, J., & Huebert, B. J. (2009). Attribution of aerosol light absorption to black carbon, brown carbon, and dust in China – Interpretations of atmospheric measurements during EAST-AIRE. *Atmospheric Chemistry and Physics*, 9(6), 2035–2050. <https://doi.org/10.5194/acp-9-2035-2009>
- Yin, Z., Wan, Y., Zhang, Y., & Wang, H. (2022). Why super sandstorm 2021 in North China? *National Science Review*, 9(3), b165. <https://doi.org/10.1093/nsr/nwab165>
- Yu, Y., Kalashnikova, O. V., Garay, M. J., & Notaro, M. (2019). Climatology of Asian dust activation and transport potential based on MISR satellite observations and trajectory analysis. *Atmospheric Chemistry and Physics*, 19(1), 363–378. <https://doi.org/10.5194/acp-19-363-2019>
- Yu, Y., Zhao, C., Kuang, Y., Tao, J., Zhao, G., Shen, C., & Xu, W. (2018). A parameterization for the light scattering enhancement factor with aerosol chemical compositions. *Atmospheric Environment*, 191, 370–377. <https://doi.org/10.1016/j.atmosenv.2018.08.016>
- Zhang, Y., Sun, Z., Chen, S., Chen, H., Guo, P., Chen, S., et al. (2021). Classification and source analysis of low-altitude aerosols in Beijing using fluorescence–Mie polarization lidar. *Optics Communications*, 479, 126417. <https://doi.org/10.1016/j.optcom.2020.126417>

References From the Supporting Information

- Alfarra, M. R., Paulsen, D., Gysel, M., Garforth, A. A., Dommen, J., Prévôt, A. S. H., et al. (2006). A mass spectrometric study of secondary organic aerosols formed from the photooxidation of anthropogenic and biogenic precursors in a reaction chamber. *Atmospheric Chemistry and Physics*, 6(12), 5279–5293. <https://doi.org/10.5194/acp-6-5279-2006>
- Bohren, C. F., & Nevitt, T. J. (1983). Absorption by a sphere: A simple approximation [software]. *Applied Optics*, 22(6), 774–775. <https://doi.org/10.1364/AO.22.000774>
- Gosse, S. F., Wang, M., Labrie, D., & Chylek, P. (1997). Imaginary part of the refractive index of sulfates and nitrates in the 0.7–2.6- μm spectral region. *Applied Optics*, 36(16), 3622–3634. <https://doi.org/10.1364/AO.36.003622>
- Hess, M., Koepke, P., & Schult, I. (1998). Optical properties of aerosols and clouds: The software package OPAC. *Bulletin of the American Meteorological Society*, 79(5), 831–844. [https://doi.org/10.1175/1520-0477\(1998\)079<0831:OPOAAC>2.0.CO;2](https://doi.org/10.1175/1520-0477(1998)079<0831:OPOAAC>2.0.CO;2)
- Li, J., Wong, J. G. D., Dobbie, J. S., & Chýlek, P. (2001). Parameterization of the optical properties of sulfate aerosols. *Journal of the Atmospheric Sciences*, 58(2), 193–209. [https://doi.org/10.1175/1520-0469\(2001\)058<0193:POTOP0>2.0.CO;2](https://doi.org/10.1175/1520-0469(2001)058<0193:POTOP0>2.0.CO;2)
- Lide, D. R. (2008). *Handbook of chemistry and physics*, 89th (InternetVersion 2009). CRC Press/Taylor and Francis.
- Liu, L., Tan, H., Fan, S., Cai, M., Xu, H., Li, F., & Chan, P. (2018). Influence of aerosol hygroscopicity and mixing state on aerosol optical properties in the Pearl River Delta region, China. *Science of the Total Environment*, 627, 1560–1571. <https://doi.org/10.1016/j.scitotenv.2018.01.199>
- Liu, X., Gu, J., Li, Y., Cheng, Y., Qu, Y., Han, T., et al. (2013). Increase of aerosol scattering by hygroscopic growth: Observation, modeling, and implications on visibility. *Atmospheric Research*, 132–133, 91–101. <https://doi.org/10.1016/j.atmosres.2013.04.007>
- Lv, M., Liu, D., Li, Z., Mao, J., Sun, Y., Wang, Z., et al. (2017). Hygroscopic growth of atmospheric aerosol particles based on lidar, radiosonde, and in situ measurements: Case studies from the Xinzhou field campaign. *Journal of Quantitative Spectroscopy and Radiative Transfer*, 188, 60–70. <https://doi.org/10.1016/j.jqsrt.2015.12.029>
- Nessler, R., Weingartner, E., & Baltensperger, U. (2005). Adaptation of dry nephelometer measurements to ambient conditions at the Jungfraujoch. *Environmental Science & Technology*, 39(7), 2219–2228. <https://doi.org/10.1021/es035450g>
- Palmer, K. F., & Williams, D. (1975). Optical constants of sulfuric acid; Application to the clouds of Venus? *Applied Optics*, 14(1), 208–219. <https://doi.org/10.1364/AO.14.000208>
- Petters, M. D., & Kreidenweis, S. M. (2007). A single parameter representation of hygroscopic growth and cloud condensation nucleus activity. *Atmospheric Chemistry and Physics*, 7(8), 1961–1971. <https://doi.org/10.5194/acp-7-1961-2007>
- Seinfeld, J. H., & Pandis, S. N. (2006). *Atmospheric chemistry and physics: From air pollution to climate change*. John Wiley & Sons.

- Wu, Y., Wang, X., Yan, P., Zhang, L., Tao, J., Liu, X., et al. (2017). Investigation of hygroscopic growth effect on aerosol scattering coefficient at a rural site in the southern North China Plain. *Science of the Total Environment*, 599–600, 76–84. <https://doi.org/10.1016/j.scitotenv.2017.04.194>
- Yan, P., Pan, X., Tang, J., Zhou, X., Zhang, R., & Zeng, L. (2009). Hygroscopic growth of aerosol scattering coefficient: A comparative analysis between urban and suburban sites at winter in Beijing. *Particuology*, 7(1), 52–60. <https://doi.org/10.1016/j.partic.2008.11.009>